ADVANCED MATERIALS INTERFACES
www.advmatinterfaces.de

Stick-On Large-Strain Sensors for Soft Robots

Sibo Cheng, Yashraj S. Narang, Canhui Yang, Zhigang Suo, and Robert D. Howe**

Soft robots require sensors that are soft, stretchable, and conformable to preserve their adaptivity and safety. In this work, hydrogels are successfully applied as large-strain sensors for elastomeric structures such as soft robots. Following a simple surface preparation step based on silane chemistry, prefabricated sensors are strongly bonded to elastomers via a "stick-on" procedure. This method separates the construction of the soft robot's structure and sensors, expanding the potential design space for soft robots that require integrated sensing. The adhesion strength is shown to exceed that of the hydrogel itself, and the sensor is characterized via quasi-static, fatigue, and dynamic response tests. The sensor exhibits exceptional electrical and mechanical properties: it can sense strains exceeding 400% without damage, maintain stable performance after 1500 loading cycles, and has a working bandwidth of at least 10 Hz, which is sufficient for rapidly-actuated soft robots. In addition, the hydrogel-based large-strain sensor is integrated into a soft pneumatic actuator, and the sensor effectively measures the actuator's configuration while allowing it to freely deform. This work provides "stick-on" large-strain sensors for soft robots and will enable novel functionality for wearable robots, potentially serving as a "sensing skin" through stimuli-responsive hydrogels.

1. Introduction

Soft robots surpass their rigid counterparts in simplicity, softness, and lightness, enabling cutting-edge applications where adaptation and safety are needed. These applications include pneumatic and microfluidic structures,[1–8] dielectric elastomer actuators,[9–11] shape memory alloys,[12,13] responsive hydrogels,[14,15] and living cells.[16] Among them, soft pneumatic robots have attracted attention due to their complex motion, simple control input, and low-impedance interactions. For soft pneumatic robots, sensing techniques are important to improve accuracy and functionality when grasping or manipulating objects of different shapes and sizes. However, the limitations of existing sensing capabilities greatly restrict the applications for this type of soft robot. Traditional rigid sensing components on soft robots can limit the deformation and compliance of the underlying soft robotic structure. Existing strain sensors for soft robots mainly rely on stretchable electronic conductors, either in the form of 1) elastomeric conductors, which consist of elastomers embedded with conducting components such as silver nanowires, silver particles, carbon nanotubes, and graphene, or 2) liquid conductors, such as grease and liquid metal. The limitations of these sensors have been noted in previous studies. The conductivity of elastomeric conductors degrades due to contact defects between separated particles or liquid, especially under large deformation, as well as the resistance-strain hysteresis resulting from cyclic loading.[17] For liquid conductors like conductive paste, the localized plastic deformation resulting from ratcheting during cyclic loading accumulates and deteriorates conductivity as well.[18,19] The change in conductivity leads to signal drifts. In addition, liquid conductors are not biocompatible and need tight sealing to prevent oxidation and leakage, thus requiring additional technical effort. Soft actuators with integrated microchannels filled with conductive fluid have been fabricated via 3D printing.[20,21] But the intricate designs and complex manufacturing requirements dramatically increase the fabrication difficulty. It remains a major challenge to manufacture robust soft strain sensors for soft robots.[22–27]

Compared to electronic conductors, ionically conductive hydrogels can be readily used as stretchable conductors,[28–30] and have recently enabled a new family of devices called hydrogel ionotronics.[31] Both the mechanical and electrical properties of hydrogels can be tuned on demand over a wide range. For example, hydrogels can be as soft as living tissues or as tough as natural rubber. As another example, the resistivity of hydrogels can vary from 18.2 MΩ m to 10^{-1} Ω m, depending on the type and concentration of salt.[32] In fact, hydrogels resemble ideal conductors, as their resistivity is a material

S. B. Cheng
International Center for Applied Mechanics
State Key Laboratory for Strength and Vibration of Mechanical Structures
School of Aerospace Engineering
Xi'an Jiaotong University
Xi'an, Shaanxi 710049, P. R. China

S. B. Cheng, Dr. Y. S. Narang, Dr. C. H. Yang, Prof. Z. G. Suo, Prof. R. D. Howe
John A. Paulson School of Engineering and Applied Sciences
Harvard University
Cambridge, MA 02138, USA
E-mail: suo@seas.harvard.edu; howe@seas.harvard.edu

S. B. Cheng, Dr. C. H. Yang, Prof. Z. G. Suo
Kavli Institute for Bionano Science and Technology
Harvard University
Cambridge, MA 02138, USA

Dr. C. H. Yang
Department of Mechanics and Aerospace Engineering
Southern University of Science and Technology
Shenzhen, Guangdong 518055, P. R. China

The ORCID identification number(s) for the author(s) of this article can be found under https://doi.org/10.1002/admi.201900985.

DOI: 10.1002/admi.201900985

 © 2019 WILEY-VCH Verlag GmbH & Co. KGaA, Weinheim

constant and independent of deformation. This feature holds even under large strain and makes hydrogels ideally suitable as large-strain sensors for soft robots.[33–38]

Nevertheless, the use of hydrogels as conductors for soft robots encounters two issues: dehydration of the hydrogel and poor adhesion between the hydrogel and the elastomer. The dehydration issue can be resolved by dissolving hygroscopic salts or encapsulating the hydrogels with low-permeability hydrophobic elastomers.[39–42] Regarding adhesion, hydrogels and elastomers are very dissimilar materials, and the adhesion between the two materials is inherently low, typically below 1 J m^{-2}. Such low adhesion does not allow measurement of the large deformation of soft robots, given that hydrogels are easily detached from elastomers. Whereas intense efforts have been devoted to resolve the adhesion issue, current strategies are limited in several aspects: surface treatment and molding are required,[41] a specific prepared glue is used,[43] or the bulk properties of the elastomers are completely altered using chemical modification.[44] Finding a new strategy to bond hydrogels with elastomers can enable hydrogel-based soft-strain sensors, improving configuration control of soft robots.

In this paper, we propose a facile "stick-on" method to achieve strong adhesion between hydrogels and elastomers without interfering with the bulk properties of elastomer; this method is based on a silane chemistry mechanism.[44] Given a preformed elastomer, we first coat the surface with a thin layer of elastomer with identical chemistry but modified with silanes such that the bulk of the elastomer maintains its original properties. We then stick a piece of hydrogel that is also modified with silanes onto the surface of the elastomer. After condensation, the silanes on the two materials form covalent siloxane bonds. We fabricate a large-strain sensor by bonding a layer of hydrogel onto an elastomer substrate and characterize the sensor via a quasistatic test, long-term fatigue test, and dynamic test. We show that the sensor can sense large strains without delamination between the hydrogel and elastomer, maintain stable performance during cyclic loading over 1500 cycles, and exhibit a bandwidth from static up to 10 Hz that is sufficient for most applications of soft robots. Finally, we validate the application of these stick-on sensors to soft robots by integrating a hydrogel sensor with a soft pneumatic actuator. We demonstrate that the hydrogel sensor can effectively measure the bending angle of the actuator throughout inflation process without interfering with deformation. The experimental results substantiate the use of hydrogels as large-strain sensors on soft robots. This work not only enables configuration control of these soft robots, but promotes the development of wearable devices that leverage strain-, chemical-, or temperature-responsive gels to achieve bionic functionality.

2. Results and Discussion

2.1. Material Synthesis and Mechanism

We first synthesize the hydrogel by copolymerizing silanes, (3-(trimethoxysilyl)propyl methacrylate (TMSPMA)), with acrylamide (AAm) (**Figure 1**a). After curing under UV for 1 h, silanes are incorporated onto the polyacrylamide (PAAm) chains. The pH of the hydrogel is tuned to 3.5 so that the silanol groups do not condense immediately after polymerization.[44] Lithium chloride, a hygroscopic salt, is used at a concentration of 8.0 M to enhance the conductivity of the hydrogel and prevent it from drying out.[39] We then bond the silane-modified hydrogel with elastomer via a stick-on strategy (Figure 1b). Unless otherwise specified, the elastomer used in this work is highly compliant silicone rubber (Ecoflex 00-30, Smooth-On, Inc., Macungie, PA). Given a prefabricated elastomer, we coat its surface with a thin layer of the same elastomer modified with silane. The polymer chains of the silane-modified elastomer can penetrate into and entangle with the preformed elastomer due to their identical chemistry, causing topological adhesion. After curing of the silane-modified elastomer, we then attach the silane-modified hydrogel onto the surface. After curing at 65 C for 24 h, silanes on the hydrogel network and elastomer network condense with each other to form siloxane bonds. The thin layer of silane-modified elastomer serves as a link, connecting the prefabricated elastomer topologically and simultaneously bonding to the hydrogel covalently.

Note that during fabrication, we only modify the surface of the elastomer; thus, the bulk properties of the elastomer are preserved. We also do not directly synthesize the hydrogel on the elastomer surface, which can be technically difficult. Instead, we make the hydrogel and elastomer separately and then stick them together. The strong but sparse inter-network siloxane bonds enable strong adhesion between the hydrogel and elastomer without hardening them. This stick-on strategy greatly simplifies the fabrication of hydrogel/elastomer hybrids and is beneficial for making hydrogels as sensors for elastomeric robots, in which the elastomers are prefabricated, the bulk properties have already been optimized, and the geometries are frequently complex.

In order to evaluate the bonding between the hydrogel and elastomer, we test the adhesion energy between the two materials using 90° peeling tests (Figure S1, Supporting Information). Typical force-displacement curves (Figure 1c) show an adhesion energy of about 60 J m^{-2}. During the peeling, cohesive fracture occurs, cracks propagate in the hydrogel, and hydrogel residues are observed on both the elastomer and the backing layer (Figure 1c, inset). The hydrogel does not detach from the elastomer surface even when the hydrogel breaks, indicating that the adhesion energy is higher than the toughness of the hydrogel. To demonstrate the notable combination of adhesion and stretchability, a fully transparent hydrogel is patterned on a 2 mm thick transparent elastomer, and the bilayer is stretched to more than twice its original length without debonding between the hydrogel and elastomer (Figure 1d).

2.2. Measurement Analysis and Quasistatic Behavior of Sensors

To validate the feasibility of using hydrogels as large-strain sensors for soft robots, we carried out quasistatic tests on hydrogel sensors. In a testing sample, hydrogel is made into a dumbbell shape and bonded to a rectangular elastomer substrate (**Figure 2**a). The two ends of the hydrogel are in contact with two strips of silver fabric to connect to an external measuring circuit. The two ends of the overall structure are confined by

© 2019 WILEY-VCH Verlag GmbH & Co. KGaA, Weinheim

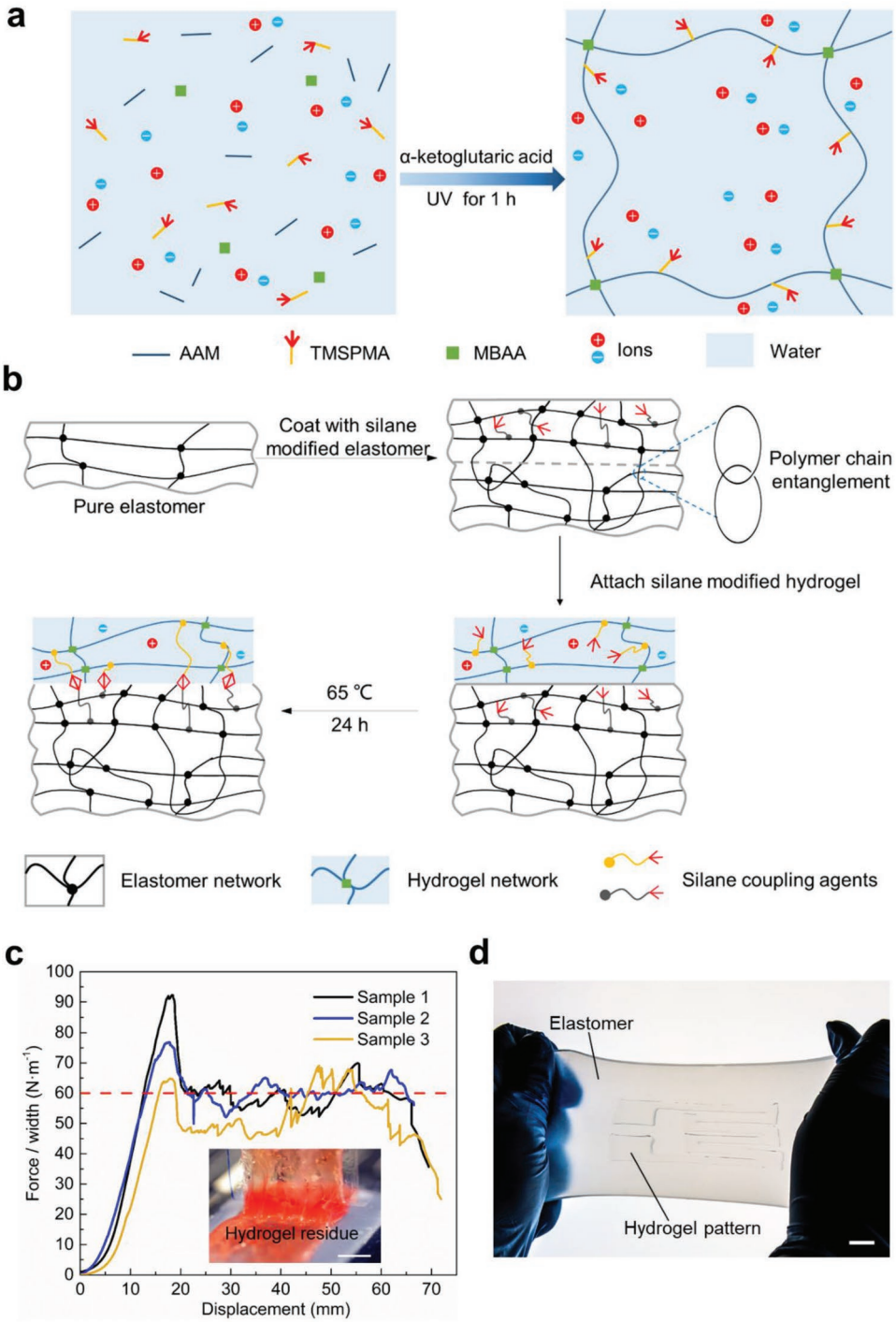

Figure 1. Synthesis, integration, and adhesion of hydrogel and elastomer. a) Hydrogel is synthesized via random copolymerization of acrylamide (AAm) and 3-(trimethoxysilyl)propyl methacrylate (TMSPMA). N,N'-methylenebis (acrylamide) (MBAA) is used as the crosslinker and α-ketoglutaric acid is used as the photoinitiator. b) Integration of hydrogel and elastomer. After standard preparation of the elastomer, its surface is coated with a thin layer of silane-modified elastomer such that the bulk of the elastomer maintains its original composition while the surface of the elastomer contains silanes. After curing, a piece of silane-modified hydrogel is simply placed on the surface (i.e., a "stick-on" process). The hydrogel is infused with salt to enhance conductivity and water retention capacity. After 24 h at 65 °C, the silanes on the hydrogel network and elastomer network form siloxane bonds to covalently bond the two networks. c) Adhesion. Typical force–displacement curves measured by 90° peeling tests. The hydrogel is TMSPMA-modified PAAm hydrogel containing 8.0 M lithium chloride. The elastomer is triethoxyvinylsilane (TEVS)-modified elastomer. The average adhesion energy is about 60 J m^{-2}. Inset: photo of a sample during a test. A crack propagates through the hydrogel (red-colored), and hydrogel residues can be observed on both the elastomer substrate and the backing layer, indicating strong adhesion between hydrogel and elastomer. d) Demonstration of a patterned transparent TMSPMA-modified PAAm hydrogel on a TEVS-modified elastomer. The bilayer is stretched to more than twice its original length without debonding between the hydrogel and elastomer. Scale bar: 1 cm.

 © 2019 WILEY-VCH Verlag GmbH & Co. KGaA, Weinheim

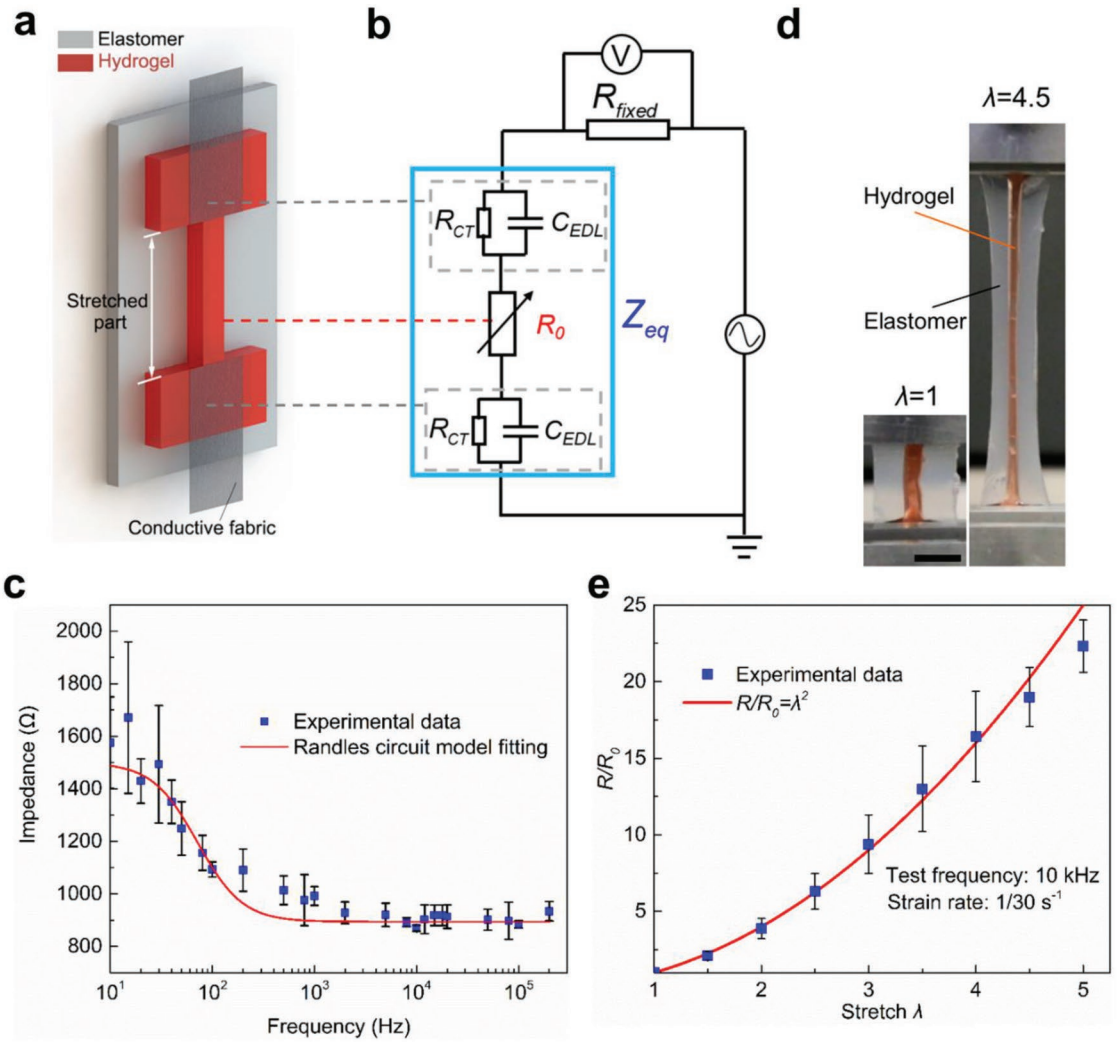

Figure 2. Quasistatic characterization of the hydrogel-based large-strain sensor. a) Schematic of the testing sample. A dumbbell-shaped hydrogel is bonded to a rectangular-shaped elastomer. The two ends of the hydrogel are connected to a measuring instrument via strips of conductive silver fabric. Note that the two ends of the sample are constrained such that only the slender part is elongated during the stretching. b) The components of the sensor correspond to analogous components of an equivalent circuit. Each interface between the hydrogel and the silver conductive fabric forms an electric double layer (EDL), which behaves like a capacitor C_{EDL} and a charge transfer path with resistance R_{CT}. The slender part of the hydrogel behaves like a pure resistor R_0. The equivalent impedance of the sensor is denoted by Z_{eq}. The hydrogel-based large-strain sensor is in series with a constant resistor, R_{fixed}, and connected to an alternating voltage source. An oscilloscope is connected to measure the voltage across the constant resistor.[45–47] c) Impedance of the sensor, Z_{eq}, as a function of measuring frequency. The Randles circuit model is used to describe the equivalent impedance,[45–47] Z_{eq}, of the sensor. The theoretical result predicted by the Randles circuit model closely approximates experimental data. The impedance approaches a constant value beyond 1 kHz. d) Photos of the sensor before and after stretch. No debonding is observed during the stretching process. Scale bar: 10 mm. e) The change of resistance of the slender part of the sensor as the sample is stretched. The measuring frequency is fixed at 10 kHz to eliminate the contribution of electric double layers, such that the impedance is dominated by the resistance of the slender part, $|Z_{eq}|\sim R_0$. The red solid line represents the relationship between resistance and stretch for an ideal incompressible conductor, for which the resistivity and volume are independent of stretch. When such a conductor is stretched to λ times its original length, its cross-sectional area is reduced by a factor of λ. Consequently, the ratio of the resistance of the stretched conductor (R) to that of the undeformed conductor (R_0) is $R/R_0 = \lambda^2$.

rigid acrylic sheets in order to ensure that the electrical connection is stable and that only the slender part of the hydrogel is stretched. In an equivalent circuit (Figure 2b), the slender part of the hydrogel is modeled as a pure resistance, R_0, and the end of the hydrogel is modeled by using the Randles circuit model,[45–47] namely a capacitor, C_{EDL}, in parallel with a resistor, R_{CT}. Here C_{EDL} is attributed to the electric double layer (EDL) forming at the interface between the ionic conductor (i.e., hydrogel) and the electronic conductor (i.e., silver fabric), and R_{CT} is attributed to the charge transfer resistance. A fixed resistor R_{fixed} is in series and connects to an alternating voltage source. The amplitude of the testing voltage is restricted to 1 V so that the EDLs will behave like capacitors without breakdown.[48]

For the EDL, charges are separated at an atomic distance; thus, the capacitance per unit area, C_{EDL}, is large, on the order of 10^{-1} F m^{-2}.[49] The area of the EDL, A_{EDL}, in our experiment is on the order of 10^{-4} m^2. For a measuring frequency, f, of

© 2019 WILEY-VCH Verlag GmbH & Co. KGaA, Weinheim

10 kHz, we estimate the impedance of the EDL as $X_C = \frac{1}{2\pi fC} \approx 1\Omega$, where $C = c_{EDL}A_{EDL}$. For the slender part of the hydrogel with length $l = 25$ mm, width $w = 2.5$ mm, and thickness $t = 2$ mm, we calculate the resistance as $R_0 = (\rho l)/(wt) = 500\ \Omega$ where $\rho \approx 10^{-1}\ \Omega$ m is the resistivity of the hydrogel doped with 8.0 M lithium chloride.[39] The equivalent impedance of the EDL is negligible compared to that of the slender part of the hydrogel so long as the measuring frequency is sufficiently high. The impedance of the hydrogel sensor can be calculated and measured as

$$Z_{eq} = \frac{U_{total} - U_{R_{fixed}}}{U_{R_{fixed}}} \cdot R_{fixed} \tag{1}$$

where U_{total} is the amplitude of the applied voltage and $U_{R_{fixed}}$ is the partial voltage on R_{fixed}. The relevant derivation is shown in the Supporting Information. We measure the impedance as a function of measuring frequency, and the theoretical prediction closely matches experimental data (Figure 2c). Details regarding the derivation are again provided in the Supporting Information. When the measuring frequency is higher than 1 kHz, the impedance Z_{eq} reaches a minimum and stabilizes at the resistance of the slender part of the hydrogel. Since we use a measuring frequency of 10 kHz for sensor characterization, we will use R in subsequent sections to represent the resistance of the hydrogel sensor.

Note that the stretch of a hydrogel only changes the configuration of its polymer network and water molecules, having a negligible effect on its ionic conductivity. Recall that the resistance of the slender part of the hydrogel is $R = (\rho l)/(A)$, where A is the cross-sectional area. When the hydrogel is stretched to λ times its original length, the cross-sectional area is reduced by a factor of λ due to incompressibility. As a result, the ratio of the resistance of the stretched hydrogel (R) to that of the unstretched hydrogel (R_0) is

$$R/R_0 = \lambda^2 \tag{2}$$

indicating that the ratio of resistances solely depends on the stretch. This property makes hydrogels ideal as large-strain sensors, whereas existing sensors degrade under large deformation. The experimentally measured relationship between the ratio of resistances and stretch is also consistent with the theoretical prediction by Equation (2) (Figure 2e). In addition, the gauge factor (GF) of a hydrogel strain sensor is

$$\mathrm{GF} = \frac{\Delta R/R_0}{\varepsilon} = \frac{\lambda^2 - 1}{\lambda - 1} = \lambda + 1 \tag{3}$$

where ΔR is the resistance variation of the sensor and ε is the strain. Thus, GF only depends on the deformation as well. Given the large stretchability of hydrogels, GF ranges from 2 to 6.

To verify the stretchability and adhesion stability of the hydrogel sensor, we stretch the sensor using a tensile machine and simultaneously conduct electrical measurements. The hydrogel, which has a shear modulus around 3.2 kPa (Figure S2, Supporting Information) is much softer than the elastomer, which has a shear modulus of 30 kPa.[50] A maximum stretch of ≈4.5 is achieved without debonding between the hydrogel and elastomer (Figure 2d; Movie S1, Supporting Information). This maximum stretch of 4.5 before hydrogel fracture is exceptional compared to other studies and shows that the sensor can be used to measure the deformation of soft robots undergoing very large deformations.[36,37,51]

2.3. Fatigue Testing

To examine the sensor performance over long-term use, we carry out fatigue tests to determine if the mechanical and electrical properties are stable during repeated operation. The design of the samples for the fatigue test is shown in Figure S3a (Supporting Information). Cyclic loading and unloading is applied with a maximum stretch of 2 at a strain rate of 0.066 s^{-1} (Figure S3b, Supporting Information). In order to slow down the dehydration process of the hydrogel sensor, an additional layer of elastomer is used to seal the hydrogel, and the two ends are connected to a resistance meter. During the test, the resistance is continuously monitored at a fixed measuring frequency of 10 kHz, and the stress–stretch curves are recorded. As the sensor is subject to cyclic stretch, the resistance changes accordingly and is captured by the resistance meter. The change of resistance as a function of stretch consistently matches the prediction $R/R_0 \approx \lambda^2$, and there is negligible hysteresis for over 1500 loading cycles, indicating high electrical stability (**Figure 3**a). The ratio R/R_0, where R represents the resistance of the sensor in the deformed state, nearly maintains a constant value of 4 at a stretch of 2. In addition, the stress–stretch curve of the 1500th cycle nearly replicates that of the 1st cycle (Figure 3b), indicating high mechanical stability. The maximum stress is constant around 40 kPa, and there is no significant hysteresis. Note that the mechanical stability is expected, as the bulk properties of the elastomer in the sensor have been preserved, and the elastomer has been optimized to be highly elastic and fatigue resistant.

As a comparative experiment, a fatigue test on a hydrogel-elastomer bilayer with no dehydration-resistant coating was also carried out to compare to the results with the coating (Figure S4, Supporting Information). The resistance of the hydrogel fluctuates over cyclic loading, resulting in the drift of the resistance–stretch curves (Figure S4a,b, Supporting Information). This is due to the fluctuation of the relative humidity in the environment that causes the swelling/deswelling of the hydrogel. However, the swelling/deswelling process of hydrogel relies on diffusion, and it takes 0.8 h for the hydrogel to exhibit a 20% change in resistance. For individual cycles with a time scale of 30 s, the change of water content is negligible, and the ratio R/R_0 always scales with λ^2. In particular, the ratio of the resistance at stretch 2 over the resistance in the original state remains a constant (Figure S4c, Supporting Information). These results demonstrate that sealing the hydrogel with an additional layer of elastomer helps stabilize the electrical performance of sensor, whereas the hydrogel containing lithium chloride by itself does not dry out in the open air. However, for sensors that are not sealed, we can measure still R_0 prior to use, and then use the constant value of R/R_0 to predict the current resistance R. For the unsealed sensor, we show long-term stability in mass and resistance over 10 d (Figure S5, Supporting Information). The samples are exposed

© 2019 WILEY-VCH Verlag GmbH & Co. KGaA, Weinheim

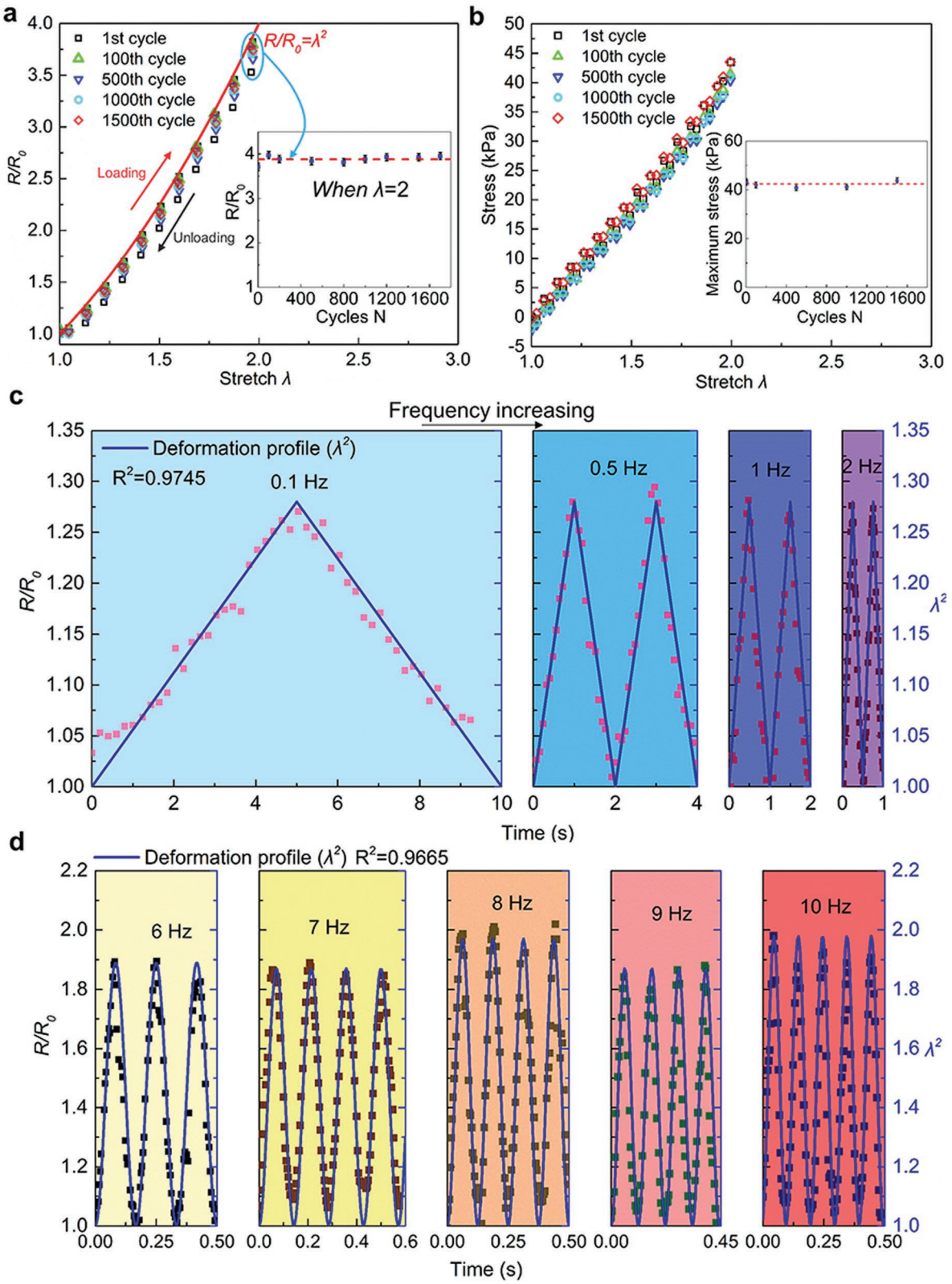

Figure 3. Dynamic characterization of the hydrogel-based large-strain sensor. a) The change of resistance as a function of stretch over repeated loading cycles. The maximum ratio of R/R_0 during each cycle is highly consistent for at least 1500 cycles, indicating stable electromechanical performance of the sensor. b) Stress–stretch curves of the sensor at different numbers of cycles. The maximum stress in each cycle remains highly consistent, indicating stable mechanical performance of the sensor. c,d) The change of resistance as a function of stretch at various loading frequencies. The electrical response closely follows the mechanical deformation.

 © 2019 WILEY-VCH Verlag GmbH & Co. KGaA, Weinheim

in an open environment with temperatures ≈20 °C and relative humidity of 20%–40%.

We note that hysteresis is often an issue in soft large-strain sensors.[17] By contrast, the hydrogel sensors exhibit negligible hysteresis. The conductivity of hydrogel comes from the movement of ions. In hydrogels, the ions are much smaller than the mesh size of the hydrogel network, so that the movement of ions is not affected by the hydrogel network. When a hydrogel sensor is deformed, the polymer network deforms while the ions are not affected. The resistance is only determined by the geometry of the hydrogel sensor. Consequently, the hydrogel sensor does not have hysteresis as long as the hydrogel is elastic. Polyacrylamide hydrogels have nearly perfect elasticity and been widely used in many hydrogel driven devices. Negligible hysteresis is observed in our experiments.

2.4. Dynamic Behavior of Sensors

In order to measure the transient deformation states of soft robots, the hydrogel sensors require a high response rate at relevant mechanical frequencies. Current pneumatically actuated soft robots typically attain a bandwidth of less than 4 or 5 Hz.[52,53] For the hydrogel sensing circuit in this work, theoretically only the RC delay limits the signal transfer time. Here the RC time constant τ is

$$\tau = RC \tag{4}$$

For our hydrogel sensor, here R is the total resistance of hydrogel sensor and C is the capacitance of EDL. Given a resistance on the order of 10^3 Ω and a capacitance on the order of 10^{-5} F, we estimate the RC delay to be on the order of 10^{-2} s. To experimentally demonstrate that performance, we conduct dynamic tests on the soft sensors at different frequencies using a universal materials testing device (model 5966, Instron, Norwood, MA) at low frequencies and a vibration platform (Hurtle Fitness Vibration Platform Workout Machine, HURVBTR30) at high frequencies. Due to limitations of the testing equipment, the stretch amplitude is not identical on both machines. However, the results at both low frequency (Figure 3c) and high frequency (Figure 3d) clearly shows the synchronization of deformation and measured resistance change from 0.1 to 10 Hz. As expected, R/R_0 is still equal to λ^2 for each frequency, indicating that the resistivity of the hydrogel sensor is still stable in the high-frequency deformation state. Based on these results, the hydrogel sensor can effectively meet the demands of most current soft robotic applications, and sensor resistance and capacitance can be controlled through geometric design to provide orders-of-magnitude increased bandwidth, if needed.

2.5. Large-Strain Sensor for Soft Robots

After characterizing the performance of the hydrogel sensor in several loading conditions, we demonstrate the capabilities of the sensor on a soft pneumatic robot. The manufacturing process consists of several steps, during which the hydrogel is bonded to the elastomeric actuator via the stick-on strategy (**Figure 4**a). In the first step, a classic multichambered pneumatic soft actuator is fabricated with a compliant upper section and a stiff, strain-limiting base layer.[2,52,54] The 3D-printed mold for actuator fabrication is shown in Figure S6 (Supporting Information). We first cast and cure a multichambered upper section (Dragon Skin 20, Smooth-On, Inc., Macungie, PA), and we then pour polydimethylsiloxane (PDMS) precursor into a separate mold to serve as a strain-limiting layer. The upper section is placed on top of the PDMS layer, and the PDMS is allowed to cure. Due to similar chemistry, the polymer chains of PDMS can diffuse into and entangle with the preformed silicone elastomer. After curing, the two elastomers are firmly bonded by topological adhesion.[55]

After the soft actuator has cured, a thin layer of silane-modified elastomer is cast and cured on the top surface of the upper section. In the second step, a salt-containing silane-modified PAAm hydrogel bonded to the silane-modified elastomer layer by simply placing it on top of the layer for 24 h at 65 °C. This stick-on strategy decouples the synthesis of the elastomer and hydrogel, facilitating the fabrication process to a large extent: given a cured elastomer and hydrogel, simply apply a primer on the surface of the elastomer and then stick on the hydrogel. This method is also generic in that silane chemistry has been extensively studied for many decades and the approach can be readily applied to numerous elastomers and hydrogels.[56,57]

This application also serves to illustrate that hydrogels can not only be used as sensors, but also as soft conductive connections (i.e., ionic cables).[34] This means that the sensor and its wiring share the benefits of strong adhesion and stick-on fabrication. To integrate the cable and the sensor together on a soft actuator and eliminate significant resistance change in the ionic cable during deformation, the hydrogel is patterned in a specific geometric design (Figure S7, Supporting Information). We denote the lengths of the ionic cable and sensor as l_C, l_S respectively, and the cross-sectional areas as A_C, A_S, respectively. We assume that the length of sensor, l_s, is 10 times that of the cable, $l_S = 10\, l_C$ and the cross-sectional area of the cable is 10 times that of the sensor, $A_C = 10\, A_S$. In addition, the resistivities of the cable and sensor are the same, i.e., $\rho_C = \rho_S$. According to $R = \rho \frac{l}{A}$, the relationship of resistance between the cable and sensor is $R_C = \frac{R_S}{100}$. Thus changes in the resistance of the cable due to deformation are negligible compared to changes in the resistance of the sensor.

We built an experimental apparatus for the characterization of the sensor-integrated pneumatic actuator (Figure S8, Supporting Information). A regulated air pressure source is used to inflate the actuator, and the pressure in the actuator itself is continuously monitored by a pressure sensor. As the pneumatic actuator is inflated, the hydrogel sensor deforms and changes its resistance accordingly. Resistance variation of the hydrogel sensor is measured by a resistance meter connected to a computer that records the measurements. The deformation process of the actuator is photographed using a digital camera (EOS 70D, Canon, Tokyo, Japan), and the bending angle can be estimated by image processing. The inflation process is incremental, and at each input pressure, we wait for steady-state to be achieved. The relative resistance of hydrogel sensor rises synchronously with the pressure (Movie S2, Supporting Information). Figure 4b shows how the pneumatic actuator

© 2019 WILEY-VCH Verlag GmbH & Co. KGaA, Weinheim

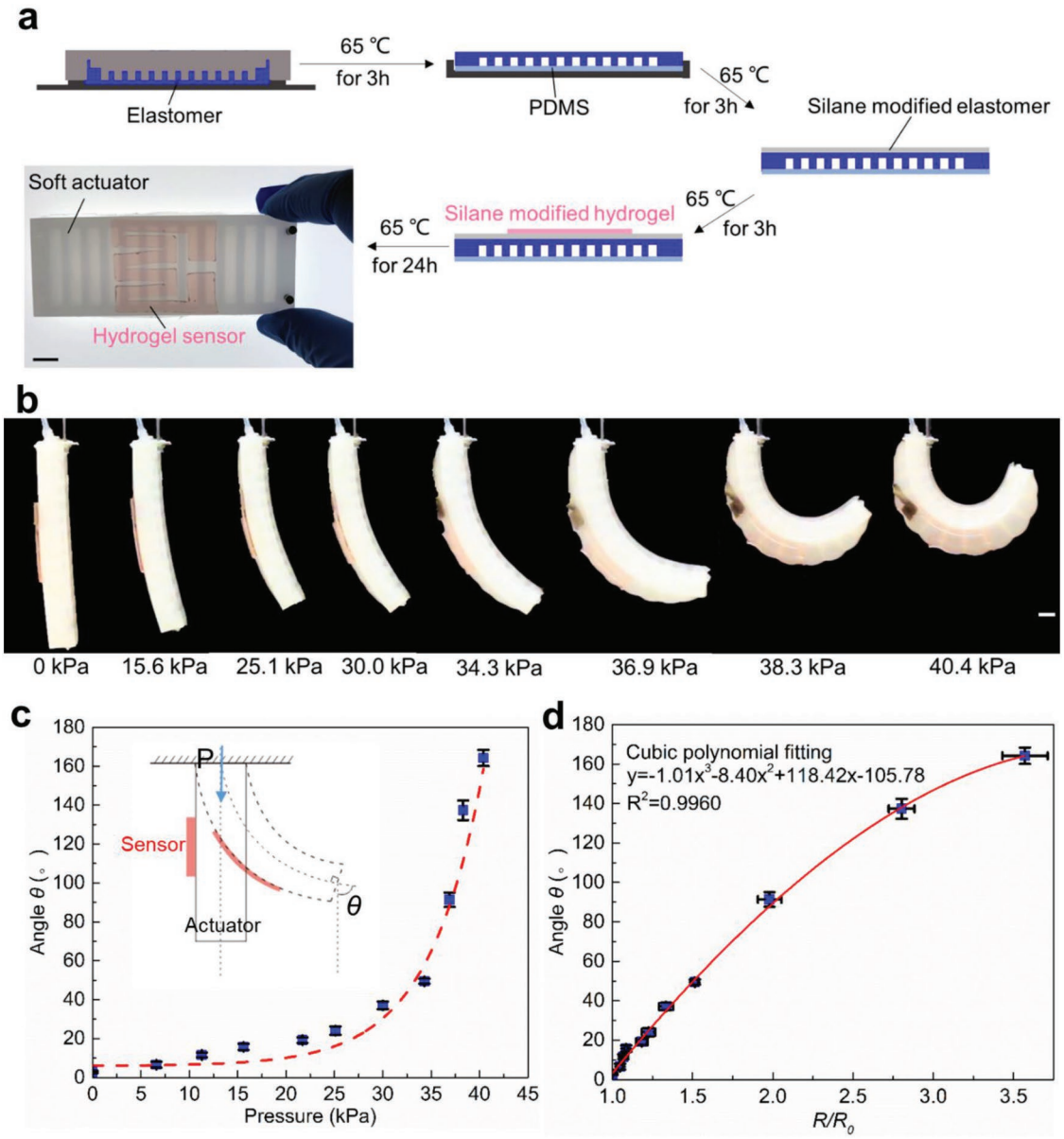

Figure 4. Stick-on large-strain sensor applied to soft robots. a) Fabrication process of a soft actuator integrated with a hydrogel-based large-strain sensor. A typical silicone rubber elastomer frame (dark blue) is synthesized by molding, followed by sealing the air chambers (white voids) with a strain-limiting layer of stiffer PDMS (pale blue) to form a pneumatic actuator. The outer surface of the actuator is then coated with a thin layer of TEVS-modified silicone rubber. Finally, a TMSPMA-modified PAAm hydrogel containing 8.0 M lithium chloride is attached and bonded to the TEVS modified silicone. The photograph shows a soft actuator integrated with a hydrogel sensor. b) A sequence of images showing the deformation process of the pneumatic actuator with increasing pressure. The red layer on the left side of the actuator is the hydrogel sensor. During the inflation process, the hydrogel sensor follows the deformation of the actuator without debonding. Scale bars: 10 mm. c) Bending angle versus pressure. The bending angle is defined as the acute angle between the centerline of the actuator and a vertical line intersecting the tip of the actuator. The red dashed line is an empirical fit. d) Bending angle as a function of relative resistance change of the hydrogel sensor. The red solid line is a cubic curve fit to the data.

deforms as the pressure increases. During the inflation process, the hydrogel sensor deforms freely with the actuator without debonding. The bending angle, θ, defined as illustrated, increases with rising pressure; a schematic of the two variables is shown in Figure 4c. The angle increases slightly at the beginning, and after a critical point, it rises rapidly with a small pressure increase. This snap-through instability is similar to inflating a balloon, as the volume keeps increasing while the pressure remains almost constant.[58] In our experiment, this critical pressure is observed to be about 38 kPa (Figure S9, Supporting Information). We note some deviations of bending angle, which are primarily due to the manual measurement technique. More precise techniques (e.g., position-tracking sensors) can be used to minimize the deviation. To predict the bending angle in an actual application, the relationship between the resistance change and angle can be accurately approximated

© 2019 WILEY-VCH Verlag GmbH & Co. KGaA, Weinheim

by a simple cubic polynomial function (Figure 4d). In practice, this fitting function can be determined by a single calibration step, after which the configuration of the pneumatic actuator can be determined by sensing resistance.

3. Discussion

This paper presents a novel hydrogel sensor technology that can be easily bonded to elastomer structures. These low-cost sensors can be readily applied to prefabricated soft robots composed of arbitrary elastomeric materials in arbitrary shapes. This decouples sensor and robot construction, simplifying the robot design process and potentially increasing the range of feasible robot configurations.

The sensor attachment process requires only application of thin silane-containing layers to the hydrogel and to the elastomer, then the sensor is simply placed on the elastomer and cured. This simple stick-on attachment of prefabricated sensors is analogous to mounting metal foil and silicon strain gauges on conventional rigid robot structures, although the attachment process is perhaps less demanding than the surface preparation required for effective strain gauge bonding.[59] Whereas we have used a 24 h heating process to generate adhesion, the kinetics of silane condensation can be accelerated by tuning variables such as pH and temperature. In addition, other coupling chemistries with faster kinetics can be used (e.g., hydrogen bonds and iron-carboxyl coordinations).

Mechanical performance is well-matched to the sensing requirements for highly compliant soft robots. Sensor stiffness can be far lower than the elastomer structure's stiffness, so that the sensors do not affect robot behavior. Tests show that complete adhesion between the sensor and elastomer persists for strains of 400%. Experiments show no evidence of delamination over 1500 strain cycles; at the end of these tests there was no discernable change in sensor response (Figure 3a,b), suggesting that wear effects may not appear for significant additional cycling. Even though the absolute resistance value of hydrogels can fluctuate with humidity and temperature, the relative change of resistance due to deformation is independent of environmental factors, indicating that a simple calibration can be occasionally performed to compensate.

Soft robots often undergo inhomogeneous deformation, exerting nonuniform load, and deformation on soft sensors. Whereas high-resolution strain mapping and high-gauge-factor nanoscale materials (e.g., single-crystal silicon nanomembranes) have been developed to meet this challenge,[60] the complex implementation and fabrication processes may hinder their widespread application. Alternatively, hydrogel sensors provide the advantage of low barrier-of-entry. When the inhomogeneous deformation cannot be mapped by one hydrogel sensor, a distributed hydrogel sensor array can be made to help sense localized strain and estimate deformation in various directions. Both stretchable electronic sensors and hydrogel sensors will find different applications that take advantage of their distinct attributes.

This paper explores only a limited range of the sensors that can be fabricated using this technology through variation in materials and geometry. Hydrogel stretchability and conductivity can be readily controlled through crosslink density and salt content. When biocompatibility becomes a concern, biocompatible hydrogel sensors can be made by using biocompatible salts, aqueous solution (e.g., phosphate-buffered saline), biocompatible ionic liquid, or biocompatible polyelectrolytes (e.g., natural polymers such as hyaluronan and chitosan).[61] Silanes can be used with a wide range of elastomers and hydrogels, so sensors can be designed with a spectrum of properties. In addition, changes in sensor geometry enables control of sensitivity and bandwidth. Hydrogels can also provide a variety of transduction mechanisms, including capacitive as well as resistive sensing. This means that in addition to strain-based pressure and curvature sensing, hydrogel sensors can be designed to respond to temperature, ion and gas species, and electric fields.[62–65]

The hydrogel adhesion technology presented here also enables the creation of integrated sensing systems. As demonstrated with the pneumatic soft robot sensor in Section 2.5, hydrogel ionic cables can form electrical connections between sensing elements that have negligible response to mechanical deformations (Figure S7, Supporting Information). Thus networks of sensors and cables can be fabricated in a single molding operation which is then bonded to the elastomer structure. This can provide low-cost, easy-to-fabricate distributed sensing of soft robot deformation to measure the overall shape of the robot as it deforms due to actuation and environmental interaction. It also provides a method for fabricating a wearable sensing skin that can measure joint positions and finger contacts as well diverse physiological parameters such as skin temperature and conductance.

4. Conclusion

We present a new approach to integrating soft hydrogels as large-strain sensors on soft robots via a simple "stick-on" method, which decouples sensor and robot fabrication. Experiments demonstrate excellent properties under the relevant operating conditions for elastomeric soft robots, including low mechanical stiffness and full adhesion between the sensor and elastomer structure through very large deformations and repeated strain cycles. The hydrogel sensor is low cost, highly transparent, and can be readily integrated with prefabricated actuators. Sensor properties and response can be varied over a wide range through materials selection and geometric design. In addition, hydrogel sensors can be adapted to wearable robots to detect physiological properties such as temperature-, ion-, and gas-activated responses. This work provides a simple, novel alternative to constructing soft sensors for numerous applications in soft robotics.

5. Experimental Section

Materials: AAm (A8887), lithium chloride (LiCl, 310 468), N,N′-methylenebisacrylamide (MBAA, M7279), α-ketoglutaric acid (75 890), 2-hydroxy-4′-(2-hydroxyethoxy)-2-methylpropiophenone (Iragcure2959, 410 896), ethyl alcohol (459 844), and TMSPMA (440 159) were purchased from Sigma-Aldrich (St. Louis, MO). PDMS (Sylgard 184) was purchased from Dow Corning (Midland, MI). Ecoflex 00-30 and

© 2019 WILEY-VCH Verlag GmbH & Co. KGaA, Weinheim

Dragon Skin were purchased from Smooth-On, Inc. (Macungie, PA). All the adapters, screws, nuts, tubes, and acrylic sheets were purchased from McMaster-Carr (Elmhurst, IL). All materials were used as received.

Synthesis of Hydrogel: For every 1 mL solution, 2.0 M of acrylamide and 8.0 M of lithium chloride were dissolved in distilled water. Then 4µL of MBAA at 0.1 M, 20 µL of α-ketoglutaric acid at 0.1 M, and 1.9 µL of 3-(trimethoxysilyl)propyl methacrylate were added. The precursor was stirred for 1 min and the solution was poured into a mold with dimensions 25 mm × 2.5 mm × 3 mm. The mold was made of acrylic sheet cut with a laser cutter (Helix 24 Laser, Epilog, Golden, CO) and assembled using cyanoacrylate glue (KG925, Krazy Glue, High Point, NC). After exposing to UV (15 W 365 nm; UVP XX-15L, 2 cm distance between sample and lamp) for 1 h, the precursor was transformed to gel.

Synthesis of Silicone Rubber: Ecoflex 00-30/Dragon Skin 20 rubber precursor was prepared by mixing the base and curing agent at a weight ratio of 1:1. After mixing and degassing in a mixer (Thinky ARE-250, Laguna Hills, CA), a homogeneous and bubble-free precursor was obtained. Then the precursor was cast into a mold with dimensions 40 mm × 4 mm × 1.5 mm and cured it at 65 °C for 2 h.

Soft Actuator Coated with a Thin Layer of Silane-Modified Elastomer: The soft actuator was fabricated via molding (Figure 4). After the actuator fabrication, a silane-modified elastomer precursor containing triethoxyvinylsilane (TEVS) (0.2 wt%) was then coated onto the surface of the actuator with the thickness around hundred micrometer. After curing at 65 °C for 2 h, the actuator was coated with a thin layer of silane-modified elastomer. Note that the silane-modified layer will not debond from the upper section of the actuator during inflation if the bonding surfaces are clean.

Adhesion Process Between Hydrogel and Elastomer: After the synthesis of the hydrogel and elastomer, the hydrogel was simply placed onto the surface of elastomer. The bilayer was then placed in an oven at 65 °C for 24 h.

Fabrication of Pneumatic Actuator: The molds were 3D-printed (Objet Connex 500 3D, Stratasys, Eden Prairie, MN, USA), as shown in Figure S6 (Supporting Information). Then Dragon Skin 20 precursor was cast into the outer mold of multichambered upper section and sealed it with the inner mold. After curing, the Dragon Skin 20 unit was moved to the mold for casting of the strain-limiting PDMS base layer.

Synthesis of Sensing Circuit on Soft Actuator: For every 1 mL solution, 2.0 M of acrylamide was dissolved and added 10 µL of acetic acid at 0.1 M, 4 µL of MBAA at 0.1 M, 1.9 µL of TMSPMA, 1 µL of Iragcure2959 at 0.1 M in ethyl alcohol. The solution was stirred for 1 min and degassed. Then the solution was poured into a mold with a specific geometric design and cured it under UV for 30 min. After curing, the hydrogel was immersed into 8.0 M LiCl aqueous solution for half an hour to allow ions to fully diffuse into the hydrogel and reached the same concentration as the solution. After that, the hydrogel was placed onto a soft actuator with a silane-modified surface. The entire structure was cured at 65 °C for 24 h to achieve stable adhesion between the hydrogel and elastomer.

Characterization of Soft Sensors: For the quasistatic, dynamic, and fatigue testing, as well as characterization of the soft robot, a stretchable silver fabric was used (Shieldex Medtex P130, V Technical Textile Inc., Palmyra, NY) to connect to the hydrogel. A waveform generator (Keysight 33512B, Keysight Technologies, Santa Rosa, CA) applied a sinusoidal voltage. The amplitude of the voltage was restricted to 1 V. An oscilloscope (Keysight DSO1004A, Keysight Technologies, Santa Rosa, CA) was used to measure the voltage across the fixed resistor that is in series with the hydrogel sensor. In the fatigue test, a resistance meter (BK Precision Model 879B, B&K Precision Corporation, Yorba Linda, CA) connected to a computer was used to measure the impedance of the sensor. For the bandwidth test at different mechanical frequencies, a dynamic test was conducted using a universal materials testing machine (Instron Model 5966, Instron, Norwood, MA) and a vibration platform (Hurtle Fitness Vibration Platform Workout Machine HURVBTR30). For pressure control and sensing, a pressure regulator (Type 90, Control Air Inc., Amherst, NH) and a pressure sensor (Vernier PS400-BTA, Vernier Software & Technology, Beaverton, OR) were used.

Supporting Information

Supporting Information is available from the Wiley Online Library or from the author.

Acknowledgements

The authors would like to thank Nikolaos Vasios from the Bertoldi Group and James Weaver, Ph.D. for their technical advice and assistance. Funding was provided by NSF National Robotics Initiative (CMMI-1637838), NSF Graduate Research Fellowship Award (DGE-1122374), NSF MRSEC (DMR-1420570), and NSF CMMI-1404653. S.B.C. was supported by the China Scholarship Council as a visiting scholar at Harvard University. This article was amended on October 23, 2019 to correct the abstract.

Conflict of Interest

The authors declare no conflict of interest.

Keywords

adhesion, hydrogel, large-strain sensor, soft robots

Received: June 4, 2019
Revised: August 1, 2019
Published online: August 28, 2019

[1] A. D. Marchese, C. D. Onal, D. Rus, *Soft Rob.* **2014**, *1*, 75.
[2] F. Ilievski, A. D. Mazzeo, R. F. Shepherd, X. Chen, G. M. Whitesides, *Angew. Chem.* **2011**, *123*, 1930.
[3] N. W. Bartlett, M. T. Tolley, J. T. Overvelde, J. C. Weaver, B. Mosadegh, K. Bertoldi, G. M. Whitesides, R. J. Wood, *Science* **2015**, *349*, 161.
[4] R. K. Katzschmann, A. D. Marchese, D. Rus, *Experimental Robotics*, Springer, Cham, Switzerland **2016**, pp. 405–420.
[5] M. Wehner, R. L. Truby, D. J. Fitzgerald, B. Mosadegh, G. M. Whitesides, J. A. Lewis, R. J. Wood, *Nature* **2016**, *536*, 451.
[6] E. T. Roche, M. A. Horvath, I. Wamala, A. Alazmani, S.-E. Song, W. Whyte, Z. Machaidze, C. J. Payne, J. C. Weaver, G. Fishbein, *Sci. Transl. Med.* **2017**, *9*, eaaf3925.
[7] A. Rafsanjani, Y. Zhang, B. Liu, S. M. Rubinstein, K. Bertoldi, *Sci. Rob.* **2018**, *3*, eaar7555.
[8] P. Rothemund, A. Ainla, L. Belding, D. J. Preston, S. Kurihara, Z. Suo, G. M. Whitesides, *Sci. Rob.* **2018**, *3*, eaar7986.
[9] F. Carpi, S. Bauer, D. De Rossi, *Science* **2010**, *330*, 1759.
[10] T. Lu, Z. Shi, Q. Shi, T. Wang, *Extreme Mech. Lett.* **2016**, *6*, 75.
[11] T. Li, G. Li, Y. Liang, T. Cheng, J. Dai, X. Yang, B. Liu, Z. Zeng, Z. Huang, Y. Luo, *Sci. Adv.* **2017**, *3*, e1602045.
[12] C. Laschi, M. Cianchetti, B. Mazzolai, L. Margheri, M. Follador, P. Dario, *Adv. Rob.* **2012**, *26*, 709.
[13] M. Cianchetti, M. Calisti, L. Margheri, M. Kuba, C. Laschi, *Bioinspiration Biomimetics* **2015**, *10*, 035003.
[14] J. Kim, J. A. Hanna, M. Byun, C. D. Santangelo, R. C. Hayward, *Science* **2012**, *335*, 1201.
[15] H. Yuk, S. Lin, C. Ma, M. Takaffoli, N. X. Fang, X. Zhao, *Nat. Commun.* **2017**, *8*, 14230.
[16] S.-J. Park, M. Gazzola, K. S. Park, S. Park, V. Di Santo, E. L. Blevins, J. U. Lind, P. H. Campbell, S. Dauth, A. K. Capulli, *Science* **2016**, *353*, 158.

 © 2019 WILEY-VCH Verlag GmbH & Co. KGaA, Weinheim

[17] L. Jin, A. Chortos, F. Lian, E. Pop, C. Linder, Z. Bao, W. Cai, *Proc. Natl. Acad. Sci. USA* **2018**, *115*, 1986.
[18] J. Huang, J. Yang, L. Jin, D. R. Clarke, Z. Suo, *Soft Matter* **2016**, *12*, 3820.
[19] X. P. Morelle, R. Bai, Z. Suo, *J. Appl. Mech.* **2017**, *84*, 101002.
[20] J. T. Muth, D. M. Vogt, R. L. Truby, Y. Mengüç, D. B. Kolesky, R. J. Wood, J. A. Lewis, *Adv. Mater.* **2014**, *26*, 6307.
[21] R. L. Truby, M. Wehner, A. K. Grosskopf, D. M. Vogt, S. G. Uzel, R. J. Wood, J. A. Lewis, *Adv. Mater.* **2018**, *30*, 1706383.
[22] Y.-L. Park, B.-R. Chen, R. J. Wood, *IEEE Sens. J.* **2012**, *12*, 2711.
[23] R. A. Bilodeau, E. L. White, R. K. Kramer, presented at *2015 IEEE/RSJ Int. Conf. on Intelligent Robots and Systems (IROS)*, IEEE, Hamburg, Germany **2015**.
[24] H. A. Wurdemann, S. Sareh, A. Shafti, Y. Noh, A. Faragasso, D. S. Chathuranga, H. Liu, S. Hirai, K. Althoefer, in *Proc. of the IEEE 37th Annual Int. Conf. on the EMBC*, IEEE, Milan, Italy **2015**.
[25] J. C. Yeo, H. K. Yap, W. Xi, Z. Wang, C. H. Yeow, C. T. Lim, *Adv. Mater. Technol.* **2016**, *1*, 1600018.
[26] S. S. Robinson, K. W. O'Brien, H. Zhao, B. N. Peele, C. M. Larson, B. C. Mac Murray, I. M. Van Meerbeek, S. N. Dunham, R. F. Shepherd, *Extreme Mech. Lett.* **2015**, *5*, 47.
[27] C. Larson, B. Peele, S. Li, S. Robinson, M. Totaro, L. Beccai, B. Mazzolai, R. Shepherd, *Science* **2016**, *351*, 1071.
[28] C. Keplinger, J.-Y. Sun, C. C. Foo, P. Rothemund, G. M. Whitesides, Z. Suo, *Science* **2013**, *341*, 984.
[29] H. Chun, T. D. Chung, *Annu. Rev. Anal. Chem.* **2015**, *8*, 441.
[30] J. Leger, M. Berggren, S. Carter, *Iontronics: Ionic Carriers in Organic Electronic Materials and Devices*, CRC Press, Boca Raton, FL **2016**.
[31] C. Yang, Z. Suo, *Nat. Rev. Mater.* **2018**, *3*, 125.
[32] R. H. Stokes, R. A. Robinson, *J. Am. Chem. Soc.* **1948**, *70*, 1870.
[33] B. Chen, Y. Bai, F. Xiang, J. Y. Sun, Y. Mei Chen, H. Wang, J. Zhou, Z. Suo, *J. Polym. Sci., Part B: Polym. Phys.* **2014**, *52*, 1055.
[34] C. H. Yang, B. Chen, J. J. Lu, J. H. Yang, J. Zhou, Y. M. Chen, Z. Suo, *Extreme Mech. Lett.* **2015**, *3*, 59.
[35] C. H. Yang, B. Chen, J. Zhou, Y. M. Chen, Z. Suo, *Adv. Mater.* **2016**, *28*, 4480.
[36] A. Frutiger, J. T. Muth, D. M. Vogt, Y. Mengüç, A. Campo, A. D. Valentine, C. J. Walsh, J. A. Lewis, *Adv. Mater.* **2015**, *27*, 2440.
[37] J. Guo, X. Liu, N. Jiang, A. K. Yetisen, H. Yuk, C. Yang, A. Khademhosseini, X. Zhao, S. H. Yun, *Adv. Mater.* **2016**, *28*, 10244.
[38] E. Acome, S. Mitchell, T. Morrissey, M. Emmett, C. Benjamin, M. King, M. Radakovitz, C. Keplinger, *Science* **2018**, *359*, 61.
[39] Y. Bai, B. Chen, F. Xiang, J. Zhou, H. Wang, Z. Suo, *Appl. Phys. Lett.* **2014**, *105*, 151903.
[40] J. Y. Sun, C. Keplinger, G. M. Whitesides, Z. Suo, *Adv. Mater.* **2014**, *26*, 7608.
[41] H. Yuk, T. Zhang, G. A. Parada, X. Liu, X. Zhao, *Nat. Commun.* **2016**, *7*, 12028.
[42] P. Le Floch, X. Yao, Q. Liu, Z. Wang, G. Nian, Y. Sun, L. Jia, Z. Suo, *ACS Appl. Mater. Interfaces* **2017**, *9*, 25542.
[43] D. Wirthl, R. Pichler, M. Drack, G. Kettlguber, R. Moser, R. Gerstmayr, F. Hartmann, E. Bradt, R. Kaltseis, C. M. Siket, *Sci. Adv.* **2017**, *3*, e1700053.
[44] Q. Liu, G. Nian, C. Yang, S. Qu, Z. Suo, *Nat. Commun.* **2018**, *9*, 846.
[45] J. E. B. Randles, *Discuss. Faraday Soc.* **1947**, *1*, 11.
[46] L. Geddes, *Ann. Biomed. Eng.* **1997**, *25*, 1.
[47] T. Shay, O. D. Velev, M. D. Dickey, *Soft Matter* **2018**, *14*, 3296.
[48] A. J. Bard, L. R. Faulkner, *Electrochemical Methods*, 2nd ed., Wiley, New York **2001**.
[49] K. H. Lee, M. S. Kang, S. Zhang, Y. Gu, T. P. Lodge, C. D. Frisbie, *Adv. Mater.* **2012**, *24*, 4457.
[50] P. Shivapooja, Q. Wang, B. Orihuela, D. Rittschof, G. P. Lopez, X. Zhao, *Adv. Mater.* **2013**, *25*, 1430.
[51] J.-B. Chossat, Y.-L. Park, R. J. Wood, V. Duchaine, *IEEE Sens. J.* **2013**, *13*, 3405.
[52] B. Mosadegh, P. Polygerinos, C. Keplinger, S. Wennstedt, R. F. Shepherd, U. Gupta, J. Shim, K. Bertoldi, C. J. Walsh, G. M. Whitesides, *Adv. Funct. Mater.* **2014**, *24*, 2163.
[53] B. Tondu, S. Ippolito, J. Guiochet, A. Daidie, *Int. J. Rob. Res.* **2005**, *24*, 257.
[54] R. F. Shepherd, A. A. Stokes, R. M. Nunes, G. M. Whitesides, *Adv. Mater.* **2013**, *25*, 6709.
[55] Z. Wang, C. Xiang, X. Yao, P. Le Floch, J. Mendez, Z. Suo, *Proc. Natl. Acad. Sci. USA* **2019**, *116*, 5967.
[56] E. P. Plueddemann, *Silane Coupling Agents*, 2nd ed., Springer, Boston, MA **1991**, p. 31.
[57] G. L. Witucki, *J. Coat. Technol.* **1993**, *65*, 57.
[58] A. Needleman, *Int. J. Solids Struct.* **1977**, *13*, 409.
[59] J. S. Wilson, *Sensor Technology Handbook*, Elsevier, Amsterdam **2004**.
[60] J. Kim, M. Lee, H. J. Shim, R. Ghaffari, H. R. Cho, D. Son, Y. H. Jung, M. Soh, C. Choi, S. Jung, *Nat. Commun.* **2014**, *5*, 5747.
[61] S. Vasiliu, M. Popa, M. Rinaudo, *Eur. Polym. J.* **2005**, *41*, 923.
[62] C. Ma, Y. Shi, D. A. Pena, L. Peng, G. Yu, *Angew. Chem.* **2015**, *127*, 7484.
[63] Y. Osada, H. Okuzaki, H. Hori, *Nature* **1992**, *355*, 242.
[64] J. Park, S. Pramanick, D. Park, J. Yeo, J. Lee, H. Lee, W. J. Kim, *Adv. Mater.* **2017**, *29*, 1702859.
[65] Z. Sun, F. Lv, L. Cao, L. Liu, Y. Zhang, Z. Lu, *Angew. Chem., Int. Ed.* **2015**, *54*, 7944.

 © 2019 WILEY-VCH Verlag GmbH & Co. KGaA, Weinheim